ELSEVIER

Materials Characterization 50 (2003) 69–79

MATERIALS CHARACTERIZATION

# Stereological estimation of the morphology distribution of ZnS clusters for photonic crystal applications

C.M. Liddell*, C.J. Summers, A.M. Gokhale

*School of Materials Science and Engineering, Georgia Institute of Technology, Atlanta, GA 30332, USA*

Received 31 January 2003; received in revised form 9 June 2003; accepted 10 June 2003

**Abstract**

A novel application of stereological methods is presented for the down selection of synthesis conditions to produce dimer building blocks for photonic crystals. Scanning electron microscopy (SEM) images of ZnS clusters were analyzed to determine the cluster population distribution for mixtures of spheres, dimers, trimers, tetramers, and other complex clusters. The volume fraction of each particle species was estimated from the average fraction of test points falling within the cluster type of interest. For example, quantitative microscopy of a particle population prepared at 29 °C for 6 h and 85 °C for 22 min yielded a composition of 59 ± 3% spheres, 31 ± 2% dimers, 7 ± 1% trimers, 0.4 ± 0.2% tetramers, and 2.5 ± 0.8% complex clusters. Images from systematically selected experimental conditions were analyzed to determine the optimal conditions for obtaining dimer building blocks from solution precipitation. This condition was determined to be 29 °C for 5 h and 85 °C for 20 min and yielded a monodispersed dimer population of 23 ± 2%.


*Keywords:* Stereological methods; ZnS clusters; Photonic crystal application

## 1. Introduction

Colloidal self-assembly has been increasingly used in science and technology areas to create nano- and mesoscale materials with dielectric properties designed to vary on the scale of light wavelengths. The class of materials with a periodic refractive index that promotes an optical band gap [1] is known as photonic crystals. Photonic crystals localize photons in microcavities [2] with spatial volumes of $\lambda^3$, inhibit spontaneous emission of excited chromophores [3], control stimulated emission in lasers [4], and allow the production of ultra-low loss waveguides [2] and ''superprisms'' [5] with especially strong dispersion characteristics. Coherent LEDs, zero-threshold semiconductor lasers [6], and enhanced optical, electronic, and quantum electronic devices are some of the important technologies enabled by the new mechanisms of light control in photonic crystals.

The width and stability of the optical band gap in a photonic crystal strongly depends on the crystal structure. As several groups [7–11] have noted, a nonspherical basis in a photonic crystal lattice promotes large photonic band gaps and is less susceptible to the disorders that may occur during colloidal self-

* Corresponding author.
*E-mail address:* gt2012@prism.gatech.edu (C.M. Liddell).

1044-5803/03/$ - see front matter © 2003 Elsevier Inc. All rights reserved.
doi:10.1016/S1044-5803(03)00103-7

assembly. Li et al. [10] proposed the face-centered cubic arrangement of nonspherical dimer building blocks to mimic the diamond structure. The diamond structure has the widest, most stable band gap but is thermodynamically impossible to form by the traditional method of self-assembly of spheres. For the proposed dimer lattice, both the asymmetry and the openness of the diamond structure are preserved. In fact, the filling fractions are identical, 34%, for dimers aligned along the <111> direction [10].

Nonspherical particles for photonic crystal bases have been produced indirectly from their spherical counterparts by thermal [12,13] and ion stretching [14,15] of spheres and by directed assembly of monodispersed [16] or binary-sized [17] spheres into complex clusters. In contrast, direct synthesis typically involves solution precipitation [18–20] methods. These methods may produce multidisperse [21] systems, having a wide range of size and shape distributions, as the stability of specific morphology classes varies strongly with the reaction conditions. Typically, ‘‘phase diagrams’’ or concentration domains [22] are presented, where the conditions that result in mixtures of various morphology types are qualitatively described.

However, the quantitative characterization of multidisperse colloidal suspensions is necessary if such systems are to be of use for photonic crystal applications. Quantitative characterization is needed to (1) determine the conditions yielding enough particles of a certain morphology class to build a lattice using the selected shape as a basis and (2) determine the conditions that produce a ‘‘dopant’’ percentage of cluster particles that, when settled along with the co-synthesized spheres, promote microcavity effects.

Few methods are available, which provide combined shape–size distributions. As an example, Manabu et al. [23] characterized ‘‘multiplets’’ of 100 nm polystyrene latex aerosol particles using a differential mobility analyzer combined with a condensation particle counter. Well-resolved concentration peaks with respect to mobility were attributed to different clusters carrying one or two units of charge. The number fraction of singlets, doublets, and triplets along with the equivalent diameter of each shape species were reported. Here, we also use a tandem technique, combining systematic point-counting stereology and quantitative scanning electron microscopy (SEM) image analysis to characterize size–shape distributions of ZnS colloidal clusters for photonic crystal applications. The quantitative measure estimated is the cluster volume fraction rather than the number fraction. Fig. 1 defines the morphology classes—sphere, dimer, trimer, tetramer, and complex cluster—synthesized and characterized quantitatively in this work. Additionally, we present the down

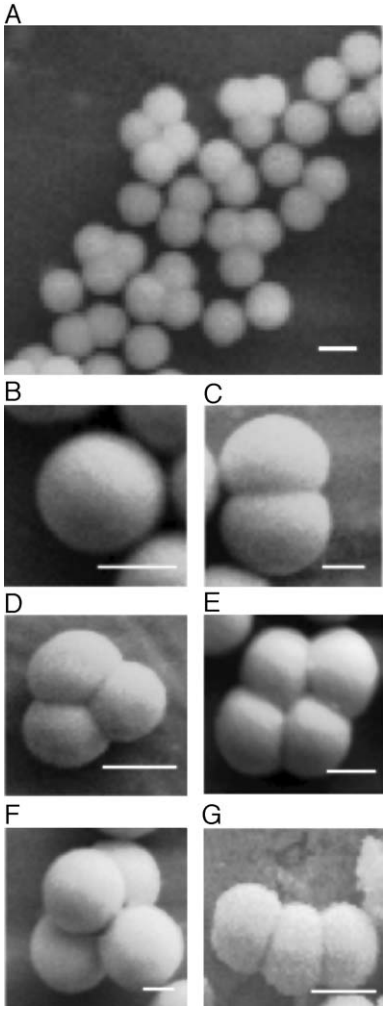


Fig. 1. SEM images of zinc sulfide colloidal clusters. (A) Mixture of morphology classes deposited from multidisperse suspension—(B) sphere, (C) dimer, (D) trimer, (E) tetramer, (F) tetrahedron, and (G) complex cluster. The category, complex cluster, is defined to include all shape varieties which do not belong to the classes shown in (B)–(E). Scale bars represent (A) 850 nm, (B) 500 nm, (C) 311 nm, (D) 667 nm, (E) 622 nm, (F) 263 nm, and (G) 1 μm.

selection of synthesis conditions for the optimum production of dimers for the diamond–analog lattice proposed by Li et al. [10]. Selection criteria on the abundance of dimers, particle size, and particle polydispersity are articulated.

## 2. Experimental

### 2.1. Materials

$Zn(NO_3)_2 \cdot 6H_2O$ (99.999%), $Mn(NO_3)_2 \cdot 4H_2O$ (99.99%), and thioacetamide (TAA, $CH_3CSNH_2$, ACS reagent grade) were purchased from Aldrich and used without further purification. Nitric acid, certified ACS plus, was obtained from Fisher. All solutions were prepared with ultrapure deionized water (18 MΩ cm).

### 2.2. ZnS particle synthesis

ZnS colloidal clusters were precipitated via a two-stage process from aqueous solutions with fixed composition—0.024 M $Zn^{2+}$, 0.00048 M $Mn^{2+}$, and 0.143 M TAA. TAA was added to the mixed cation solutions at room temperature. To control the release of sulfide ions from TAA, the solutions were acidified with $0.800 \pm 0.001$ ml of 15.8 M $HNO_3$. The reactions were carried out in 200 ml Erlenmeyer flasks sealed with laboratory film.

Primary nanocrystal seeds were produced by immersing the reaction vessels in a constant temperature water bath for 4–6 h at 26–32 °C. The seed solutions were placed in a second bath at 85 °C to grow colloidal clusters. The reactions were terminated after 20–30 min by quenching the solutions to below 10 °C in an ice bath. The combinations of seed time, seed temperature, precipitation time, and precipitation temperature used in this study are provided in the sample matrix shown in Table 1. ZnS particles were separated from the mother liquid by centrifuging and were redispersed and washed three times with water. The particles were collected by filtration on 0.22 μm cellulose ester membranes.

### 2.3. Scanning electron microscopy

Dried ZnS powders were resuspended in water and ultrasonically dispersed to insure homogeneity in the suspension and representative sampling. Several drops of ZnS suspension were placed on a bare aluminum SEM mount. Particles were allowed to settle for several minutes. The excess liquid was removed and the mount was dried under a flow of nitrogen gas. By this procedure, particles were deposited as monolayers or bilayers onto areas of the SEM mount. SEM images were obtained at 5 kV using a LEO 1530 thermally assisted FEG scanning electron microscope. High-resolution images from 10 sampling regions were obtained without gold coating the samples.

### 2.4. Point-counting stereology

The point-counting stereological method was employed to obtain volume fraction estimates for

Table 1
Sample identification matrix[a]

| Seed time (h) | Seed temperature (°C) | Precipitation temperature (°C) | Precipitation time | | | | |
|---|---|---|---|---|---|---|---|
| | | | 20 min | 22 min | 25 min | 30 min | 35 min |
| 4 | 26 | 85 | 4268520 | 4268522 | 4268525 | 4268530 | 4268535 |
| 5 | 26 | 85 | 5268520 | 5268522 | 5268525 | 5268530 | 5268535 |
| 6 | 26 | 85 | 6268520 | 6268522 | 6268525 | 6268530 | 6268535 |
| 4 | 29 | 85 | 4298520 | 4298522 | 4298525 | 4298530 | 4298535 |
| 5 | 29 | 85 | 5298520 | 5298522 | 5298525 | 5298530 | 5298535 |
| 6 | 29 | 85 | 6298520 | 6298522 | 6298525 | 6298530 | 6298535 |
| 4 | 32 | 85 | 4328520 | 4328522 | 4328525 | 4328530 | 4328535 |
| 5 | 32 | 85 | 5328520 | 5328522 | 5328525 | 5328530 | 5328535 |
| 6 | 32 | 85 | 6328520 | 6328522 | 6328525 | 6328530 | 6328535 |

[a] Sample labels reflect the reaction conditions, i.e., 4 26 85 20 refers to a sample prepared with a seed time of 4 h, seed temperature of 26 °C, precipitation temperature of 85 °C, and precipitation time of 20 min.

each morphological type in the suspension. Stereology is an unbiased statistical method used to characterize the relative number, length, surface area, and/or volume of features in a microstructure without assumptions concerning size, shape, orientation, or location of the features. In practice, it is a technique that allows the accurate estimation of three-dimensional structural parameters and their standard deviations from two-dimensional projections. In the present study, the method described by Gokhale et al. [24] was used with a modification to eliminate the effect of differences in particle concentration between SEM images.

SEM images were overlaid with a grid of 728 evenly spaced test points. The number of test points falling on a particular morphological type was counted and divided by the total number of test points falling on particles, regardless of their morphology. This ratio is defined as the point fraction ($P_P$). The point fractions of five particle types—sphere, dimer, trimer, tetramer, and complex cluster—were determined. Typically, the volume fraction ($V_V$) of each particle species was estimated by averaging $P_P$ over 10 microstructural fields. Volume fractions were calculated according to Eq. (1) and reported in terms of volume percentage.

$$V_V = \langle P_P \rangle \pm \frac{2\sqrt{S^2}}{\sqrt{N}} \tag{1}$$

where $\frac{2\sqrt{S^2}}{\sqrt{N}}$ is the sampling error in the volume fraction determination, $N$ is the total number of microstructural fields, and $S^2$ is the sample variance. The variance was calculated as follows:

$$S^2 = \frac{\sum(\langle P_P \rangle - P_{Pi})^2}{(N-1)} \tag{2}$$

where $P_{Pi}$ is the point fraction of the $i$th microstructural field ($i = 1,2,\ldots n$).

### 2.5. Image analysis: particle size measurement

The average size, standard deviation, and coefficient of variation (CV) were derived from SEM images, typically by measuring 100 spheres and 50 dimers. The diameter of spheres and longest dimension of dimers were measured. CV, the ratio of the

Table 2
Systematic point-counting stereology data for sample 5298520

| Points in spheres | Points in dimers | Points in trimers | Points in complex cluster | Points in tetramers | Total points in particles | $P_P$ sphere | $P_P$ dimer | $P_P$ trimer | $P_P$ complex cluster | $P_P$ tetramer |
|---|---|---|---|---|---|---|---|---|---|---|
| 191 | 61 | 15 | 5 | 3 | 275 | 0.6945 | 0.2218 | 0.0545 | 0.0182 | 0.0109 |
| 198 | 66 | 14 | 0 | 0 | 278 | 0.7122 | 0.2374 | 0.0504 | 0.0000 | 0.0000 |
| 258 | 86 | 15 | 4 | 0 | 363 | 0.7107 | 0.2369 | 0.0413 | 0.0110 | 0.0000 |
| 219 | 88 | 15 | 0 | 0 | 322 | 0.6801 | 0.2733 | 0.0466 | 0.0000 | 0.0000 |
| 224 | 82 | 11 | 2 | 0 | 319 | 0.7022 | 0.2571 | 0.0345 | 0.0063 | 0.0000 |
| 245 | 71 | 12 | 2 | 0 | 330 | 0.7424 | 0.2152 | 0.0364 | 0.0061 | 0.0000 |
| 243 | 53 | 2 | 2 | 0 | 300 | 0.8100 | 0.1767 | 0.0067 | 0.0067 | 0.0000 |
| 306 | 84 | 9 | 5 | 0 | 404 | 0.7574 | 0.2079 | 0.0223 | 0.0124 | 0.0000 |
| 219 | 72 | 6 | 2 | 2 | 301 | 0.7276 | 0.2392 | 0.0199 | 0.0066 | 0.0066 |
| 191 | 76 | 14 | 1 | 0 | 282 | 0.6773 | 0.2695 | 0.0496 | 0.0035 | 0.0000 |

| $S^2(n)$ | | | | | Spheres (%) | Dimers (%) | Trimers (%) | Complex clusters (%) | Tetramers (%) |
|---|---|---|---|---|---|---|---|---|---|
| Sphere | Dimer | Trimer | Complex cluster | Tetramer | | | | | |
| 0.001618 | 0.000872 | 0.000243 | 3.129e − 05 | 1.47e − 05 | 72.15 | 23.35 | 3.62 | 0.71 | 0.18 |
| | | | | | *Sampling error* | | | | |
| | | | | | 2.54% | 1.87% | 0.99% | 0.35% | 0.24% |

standard deviation to the mean of the size distribution, was used to characterize the polydispersity. For colloidal self-assembly to occur, CV must be less than ~ 10% [25].

## 3. Results and discussion

### 3.1. Morphology distributions

Table 2 provides stereology data from sample 5298520 and lists the resulting shape distribution in tabular form. For this sample, the morphology distribution by volume was $72.15 \pm 2.54\%$ spheres, $23.35 \pm 1.87\%$ dimers, $3.62 \pm 0.99\%$ trimers, $0.18 \pm 0.24\%$ tetramers, and $0.71 \pm 0.35\%$ complex clusters. Sampling from 10 microstructural fields was sufficient to reduce the relative error for percentage sphere and dimer determinations to acceptable levels $< 10\%$. However, for the less abundant, more complex morphologies, the error became quite significant. A more precise determination in these cases requires that the number of microstructural fields examined be increased. Digital image analysis would make the study of much larger numbers of microstructural fields feasible. The morphology distributions obtained from

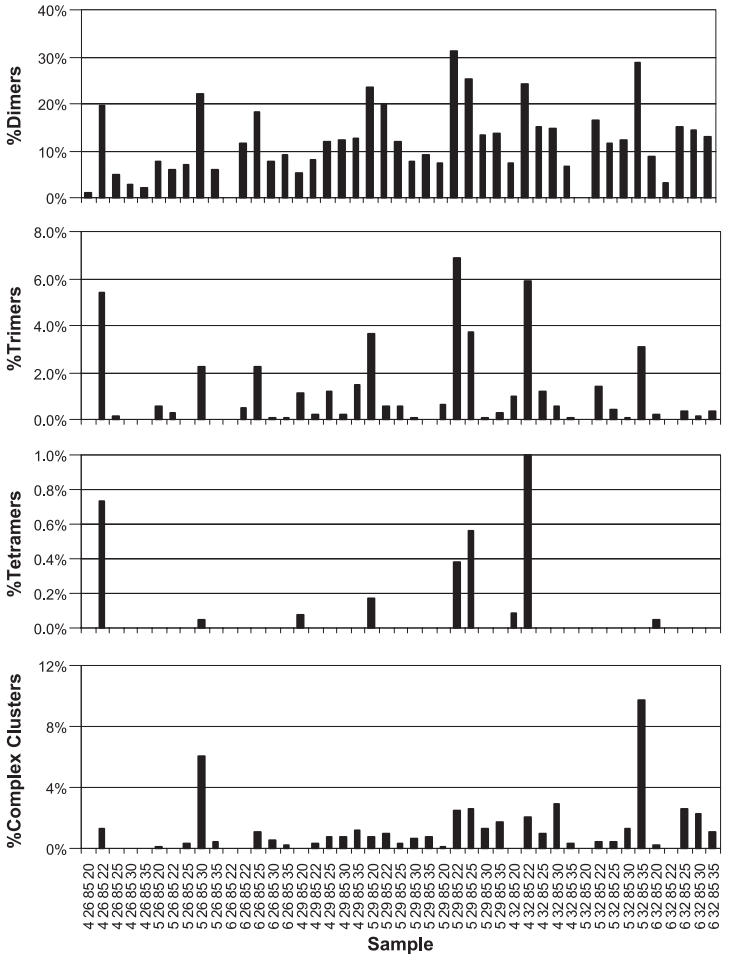


Fig. 2. Morphology distributions of ZnS colloidal clusters. Quantitative shape characterization was obtained by point-counting stereology analysis of 10 SEM fields per sample. Sample labels refer to experimental conditions: seed time (h), seed temperature (°C), precipitation temperature (°C), and precipitation time (h), respectively.

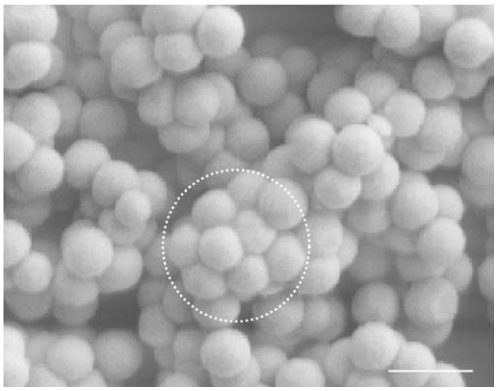

Fig. 3. SEM image of ZnS particle network. Reaction conditions included seeding for 5 h at 32 °C, incubation at room temperature for 2 days, and precipitation at 85 °C for 21 min. A close-packed floc is circled. Scale bar represents 1 μm.

all of the syntheses performed are presented graphically in Fig. 2.

Fig. 2 shows that for all except two samples, 5328535 and 5268530, the quantity of complex clusters produced remained low, less than ~ 3%. The low percentage of irregularly shaped clusters shows the viability of the present synthetic method in producing uniform clusters of each morphology class. For all conditions presented, spheres account for over half of the particles produced. Of the other well-defined morphology types, dimers are next in abundance (max 31vol.%), followed by trimers (max 7vol.%), and then tetramers (max 1vol.%). This ''stepped'' decrease in abundance may imply that clusters form by the coagulation of preexisting monodispersed spheres. This type of coagulation can occur as the volume fraction of spheres increases during colloid precipitation at elevated temperatures.

The coagulation of ceramic particles (alumina, titania, and zirconia) in high solids loading slurries has been utilized by Yang and Sigmund [26,27] to form ceramic parts by direct casting methods. Fractal models, which describe either reaction or diffusion limited cluster aggregation [28,29], as well as percolation [30] models have been proposed for such processes. Further investigations applying these models to the current system are required. We note, however, that we have observed a particle network of close packed flocs, a characteristic of late stage cluster–cluster aggregation, in the case of prolonged aging between seeding and final high temperature growth steps. Fig. 3 provides an example of the networks formed by aging the solutions for 5 h at 32 °C, incubating for 2 days at room temperature, and aging at 85 °C for 21 min.

### 3.2. Dimer maximization

Table 3 summarizes and highlights the synthesis conditions that generate the greatest percentages of dimers. The particle suspensions having greater than 20% dimer content are noted by cell shading. These conditions produce a reasonable yield of dimer particles, which can be harvested from the suspension and used as building blocks in photonic crystals or as dielectric dopants.

Generally, a seed temperature of 29–32 °C coupled with a precipitation time of 20–25 min led to

Table 3
Average percentage of dimers synthesized in multidisperse suspensions

| Seed time (h) | Seed temperature (°C) | Precipitation temperature (°C) | Precipitation time and average %dimers | | | | |
|---|---|---|---|---|---|---|---|
| | | | 20 min | 22 min | 25 min | 30 min | 35 min |
| 4 | 26 | 85 | 1.1 ± 0.2% | 20 ± 2% | 5 ± 3% | 3 ± 2% | 2.2 ± 0.9% |
| 5 | 26 | 85 | 8 ± 2% | 6.0 ± 0.9% | 7 ± 1% | 22 ± 2% | 6 ± 1% |
| 6 | 26 | 85 | – | 12.6 ± 1.2% | 18 ± 2% | 8 ± 2% | 9 ± 2% |
| 4 | 29 | 85 | 5.4 ± 0.7% | 8 ± 2% | 12 ± 2% | 12 ± 2% | 12 ± 1% |
| 5 | 29 | 85 | 23 ± 2% | 20 ± 3% | 12 ± 2% | 8 ± 1% | 9 ± 2% |
| 6 | 29 | 85 | 7 ± 2% | 31 ± 2% | 25 ± 2% | 13 ± 1% | 14 ± 1% |
| 4 | 32 | 85 | 7.3 ± 0.9% | 24 ± 2% | 15 ± 2% | 15 ± 2% | 7 ± 1% |
| 5 | 32 | 85 | – | 17 ± 3% | 12 ± 1% | 12 ± 1% | 29 ± 2% |
| 6 | 32 | 85 | 9 ± 2% | 3 ± 1% | 15 ± 2% | 14 ± 3% | 13 ± 3% |

the highest dimer yields. A higher abundance of dimers at shorter precipitation times may be explained by considering the size of the aggregating spheres. As precipitation proceeded, the spheres typically increased in size as shown in Fig. 4A. The larger size of spheres at longer precipitation times made them less susceptible to van der Waals forces and thus more stable against coagulation. When sphere size showed an atypical decrease at longer precipitation times, as in the case of samples 5268530 and 5328536, a corresponding increase in dimer abundance was observed. The particle sizes for these two samples are noted in Fig. 4B and C, respectively. As Table 3 shows, samples 5268530 and 5328535 are the only samples producing a high dimer yield among those prepared with precipitation time longer than 25 min.

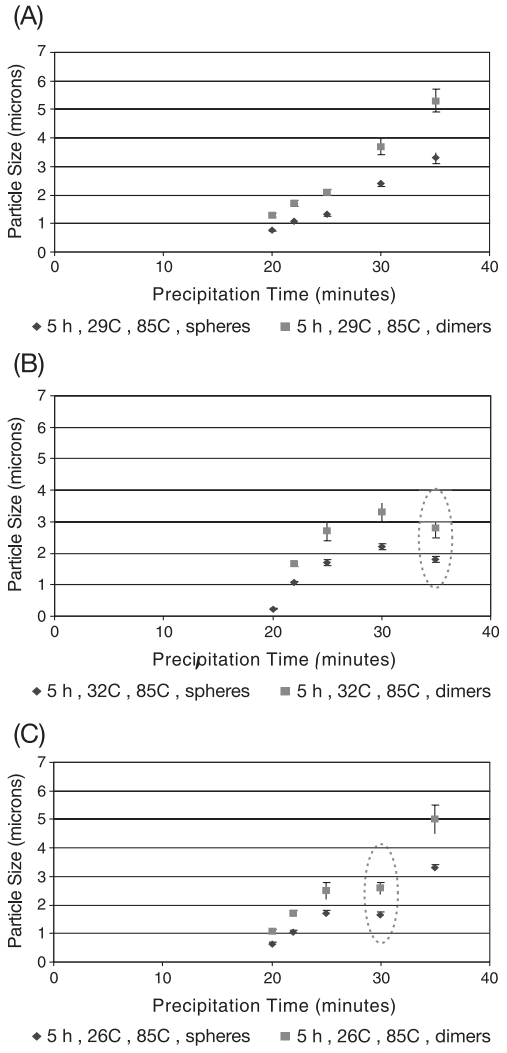


Fig. 4. Effect of precipitation time on particle size. Particle size is plotted as a function of precipitation time for samples (A) 5298520–5298535, (B) 5328520–5328535, and (C) 5268520–5268535. Particle size increases with precipitation time over the entire range illustrated in (A). (B) and (C) show an atypical decrease in particle size at longer precipitation times. The circled data correspond to samples 5328535 and 5268530, respectively.

### 3.3. Particle size and polydispersity

Particle size is an important parameter for photonic crystal applications. When colloidal particles are the building blocks in photonic crystals, the particle size determines the lattice constant of the crystal. The lattice constant is directly related to the frequency location of the photonic band gap [2]. Thus, particle size determines which frequencies of light can be expected to interact with the crystal for the observation of the unique optical properties of photonic crystals.

Fig. 5A–D shows SEM images, particle shape, and size distributions for selected samples (5298520, 5298522, 6298522, and 6298525), meeting the 20% dimer threshold and having average dimer size less than 2 μm. In optimizing the ZnS cluster synthesis conditions for photonic crystal applications, we have limited the cluster size to 2 μm so that the particles can be used for device operation in the near-IR region. However, clusters ranging from 950 nm (4298520) to 6.5 μm (4268535) were produced here. Comprehensive particle size information will be presented elsewhere.

Generally, a shorter precipitation time resulted in particles with smaller size and lower polydispersity. For each sample in Fig. 4, polydispersity was less than 10% for spheres and dimers indicating that the particles have potential for self-assembly. Sphere and dimer polydispersity values ranged from 4.74% to 7.61% and 5.67% to 7.91%, respectively.

Though the sample prepared at 29 °C for 6 h and 85 °C for 22 min produced the largest percentage of dimers, the particles prepared at 29 °C for 5 h and 85 °C for 20 min generated the smallest dimer size and size distribution, as well as fewer other cluster types. Thus, for photonic crystal applications, the latter

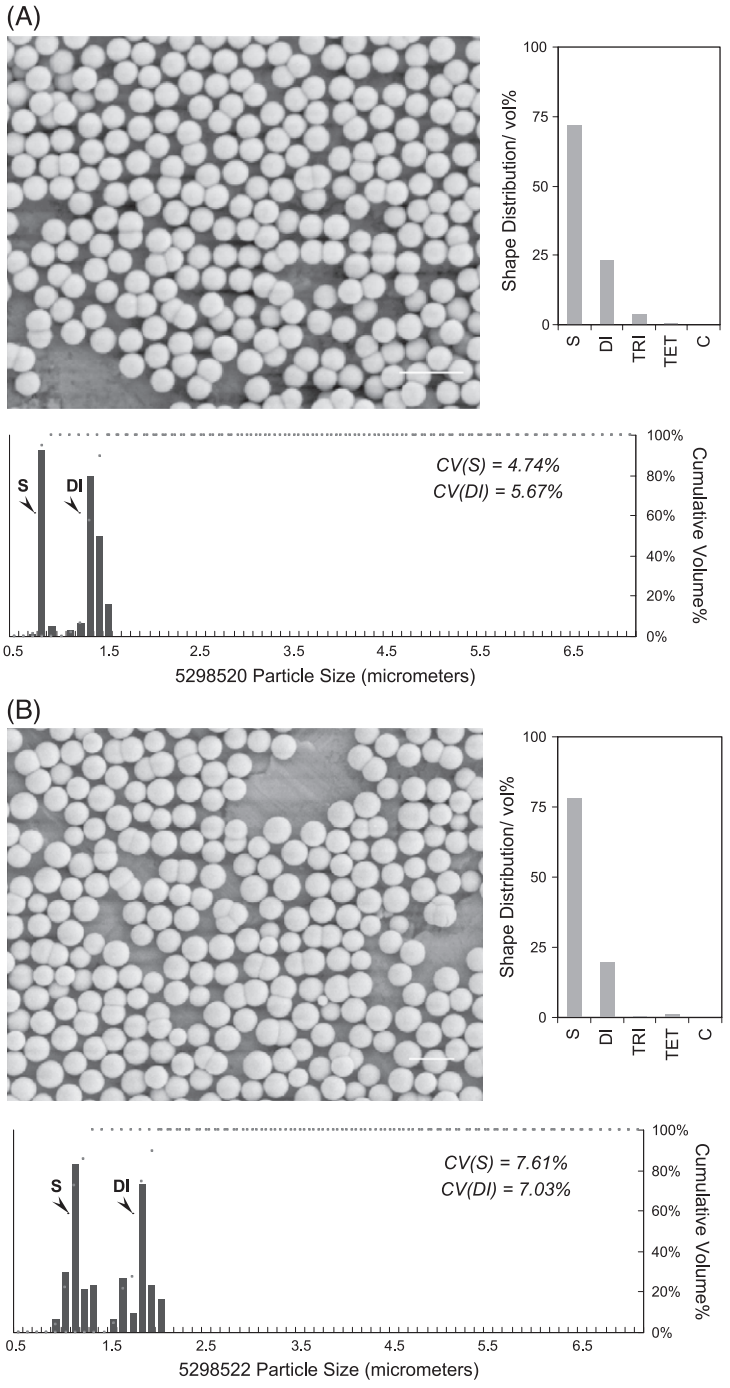


Fig. 5. ZnS particle size–shape correlation. The scanning electron micrographs, particle size distributions, and shape distributions are shown for (A) sample 5298520, (B) 5298522, (C) 6298522, and (D) 6298525. S, DI, TRI, TET, and C refer to shape classes—sphere, dimer, trimer, tetramer, and complex cluster. CV is the relative standard deviation and characterizes the polydispersity of the clusters. Scale bars represent 2 μm.

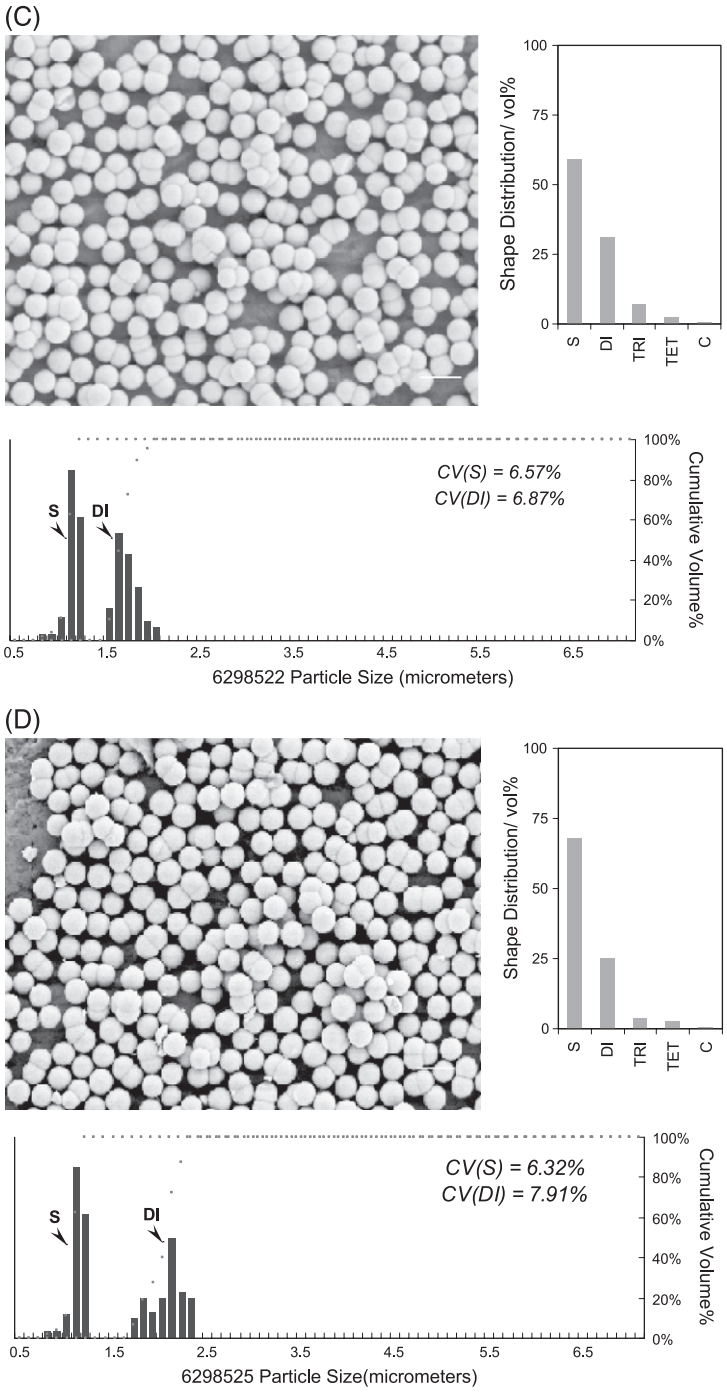


Fig. 5 (*continued*).

synthesis conditions are best suited for producing dimers that can be harvested by physical means.

## 4. Conclusion

This work demonstrates a unique application of stereological methods to the down selection of synthesis conditions for producing the morphology distributions most desirable for photonic crystal applications. Stereological methods provided quantitative characterization of the morphology distributions produced by multidisperse particle syntheses. The method is widely applicable for morphology mixtures of all material types. The tandem size–shape characterization presented is limited only by the resolution of the microscope. With the present instrumentation, colloids with particle sizes down to 1 nm may be examined.

We have shown the utility of the systematic point-counting stereology method in optimizing the conditions to produce ZnS dimer building blocks. The optimum particle system was obtained from seeds prepared at 29 °C for 5 h and aged for 20 min at 85 °C. The estimated yield of dimers was 23%, having average size 1.29 μm and polydispersity 5.67%, well within the requirements for self-assembly.

Assembly of the dimers synthesized here would promote the formation of a photonic band gap in the near-IR region. Producing ZnS clusters for photonic crystals operational in the visible region requires further synthesis design to reduce the particle size. Several groups [31–33] have made uniform ZnS spheres in the applicable size range, 200–350 nm, by techniques similar to the one discussed here. Our future work includes varying experimental parameters such as reactant concentration to prepare smaller ZnS clusters. Additionally, field flow fractionation will be utilized to perform the physical separation of the particle morphology classes.

## Acknowledgements

This work was supported in part by the Army Research Office MURI program (DAAD19-01-1-0603). C.M. Liddell thanks the Office of Naval Research for fellowship support.

## References

[1] Ho KM, Chan CT, Soukoulis CM. Photonic gaps for electromagnetic waves in periodic dielectric structures: discovery of the diamond structure. In: Soukoulis CM, editor. Photonic band gaps and localization. New York: Plenum; 1993. p. 235–45.
[2] Joannopoulos JD, Villeneuve PR, Fan S. Photonic crystals: putting a new twist on light. Nature 1997;386:143–9.
[3] Yablonovitch E. Inhibited spontaneous emission in solid state physics and electronics. Phys Rev Lett 1987;58:2059–62.
[4] Krauss TF, De la Rue RM. Photonic crystals in the optical regime—past, present, and future. Prog Quantum Electron 1999;23:51–96.
[5] Kosaka H, Kawashima T, Tomita A, Notomi M, Tamarura T, Sato T, et al. Photonic crystals for micro lightwave circuits using wavelength-dependent angular beam steering. Appl Phys Lett 1999;74:1370–2.
[6] Hirayama H, Hamano T, Aoyagi Y. Novel surface emitting laser diode using photonic band-gap crystal cavity. Appl Phys Lett 1996;69:791–3.
[7] Li ZY, Zhang ZQ. Photonic bandgaps in disordered inverse-opal photonic crystals. Adv Mater 2001;13:433–6.
[8] Li Z, Lin L, Gu B, Yang G. Photonic band gaps in anisotropic crystals. Physica, B 2000;279:159–61.
[9] Lu Y, Yin Y, Xia Y. Three-dimensional photonic crystals with non-spherical colloids as building blocks. Adv Mater 2001;13:415–20.
[10] Li Z, Wang J, Gu B. Full band gap in FCC and BCC photonic band gap structure: non-spherical atom. J Phys Soc Jpn 1998;67:3288–91.
[11] Anderson CM, Giapis KP. Symmetry reduction in group 4mm photonic crystals. Phys Rev, B 1997;56:7313–20.
[12] Lu Y, Yin Y, Xia Y. Preparation and characterization of micrometer-sized 'egg shells'. Adv Mater 2001;13:271–4.
[13] Peng J, Bertone JF, Colvin VL. A lost-wax approach to monodisperse colloids and their crystals. Science 2001;291:453–7.
[14] Snoeks E, van Blaaderen A, van Dillen T, van Kats CM, Velikov K, Brogersma ML, et al. Colloidal assemblies modified by ion irradiation. Nucl Instrum Methods, B 2001;178:62–8.
[15] Snoeks E, van Blaaderen A, van Dillen T, van Kats CM, Velikov K, Brogersma ML, et al. Colloidal ellipsoids with continuously variable shape. Adv Mater 2001;12:1511–4.
[16] Yin Y, Xia Y. Self-assembly of monodispersed spherical colloids into complex aggregates with well-defined sizes, shapes, and structures. Adv Mater 2001;13:267–70.
[17] Yin Y, Lu Y, Xia Y. A self-assembly approach to the formation of asymmetric dimers from monodispersed spherical colloids. J Am Chem Soc 2001;123:771–2.
[18] Wang Y, Muramatsu A, Sugimoto T. FTIR analysis of well-defined $\alpha$-$Fe_2$-$O_3$ particles. Colloids Surf, A 1998;134:281–97.
[19] Matijevic E. Preparation and properties of uniform size colloids. Chem Mater 1993;5:412–26.
[20] Matijevic E. Uniform inorganic colloid dispersions. Achievements and challenges. Langmuir 1994;10:8–16.
[21] Sahagian DL, Proussevitch AA. 3D particle size distributions from 2D observations: stereology for natural applications. J Volcanol Geotherm Res 1998;84:173–96.

[22] Matijevic E, Cimas S. Formation of uniform colloidal iron (III) oxides in ethylene glycol–water solutions. Colloid Polym Sci 1987;265:155–63.
[23] Manabu S, Chang H, Fujishige Y, Okuyama K. Calibration of polarization-sensitive and dual-angle laser light scattering methods using standard latex particles. J Colloid Interface Sci 2001;241:71–80.
[24] Gokhale AM, Drury WJ, Whited B. Quantitative microstructural analysis of anisotropic materials. Mater Charact 1993;31: 11–7.
[25] Rakers S, Chi LF, Fuchs H. Influence of the evaporation rate on the packing order of polydisperse latex monofilms. Langmuir 1997;13:7121–4.
[26] Yang Y, Sigmund WM. Preparation, characterization, and gelation of temperature induced forming (TIF) alumina slurries. J Mater Synth Process 2001;9:103–9.
[27] Yang Y, Sigmund WM. Effect of particle volume fraction on the gelation behavior of the temperature induced forming (TIF) aqueous alumina suspensions. J Am Ceram Soc 2001;84: 2138–40.
[28] Odriozola G, Tirado-Mirando M, Schmitt A, Martinez Lopez F, Callejas-Fernandez J, Martinez-Garcia R, et al. J Colloid Interface Sci 2001;240:90–6.
[29] Mellema M, van Opheusden JHJ, van Vilet T. Relating colloidal particle interactions to gel structure using Brownian dynamics simulations and the Fuchs stability ratio. J Chem Phys 1999;111:6129–35.
[30] Yang Y, Sigmund WM. Expanded percolation theory model for the temperature induced forming (TIF) of alumina aqueous suspensions. J Eur Ceram Soc 2002;22:1791–9.
[31] Tian Y, Dinsmore AD, Qadri SB, Ratna BR. Microsized structures fabricated with nanoparticles as building blocks. Mater Res Soc Symp Proc 1999;536:205–9.
[32] Velikov KP, van Blaaderen A. Synthesis and characterization of monodisperse core-shell colloidal spheres of zinc sulfide and silica. Langmuir 2001;17:4779–86.
[33] Wilhelmy DM, Matijevic E. Preparation and properties of monodispersed spherical–colloidal particles of zinc sulphide. J Chem Soc, Faraday Trans 1984;80:563–70.